International Journal of Environmental Science and Technology (2023) 20:4203–4218
https://doi.org/10.1007/s13762-022-04249-x

ORIGINAL PAPER

Polyhedral magnetite nanoparticles modified with porous bio-templated copper oxide as catalyst for visible-light-driven photodegradation of methylene blue

O. A. Alani[1] · H. A. Ari[1,2] · S. O. Alani[3] · N.-A. O. Offiong[1,4] · W. Feng[1]

Received: 1 June 2021 / Revised: 4 February 2022 / Accepted: 12 April 2022 / Published online: 19 May 2022

Abstract

A visible-light-driven bio-templated magnetic copper oxide ($CuO/C/Fe_3O_4$) photocatalyst was prepared via modifying polyhedral magnetite nanoparticles with porous bio-templated copper oxide for the heterogeneous photo-Fenton degradation of methylene blue illuminated by visible light. The synthesized composite was subsequently characterized by X-ray diffraction analysis, thermally gravimetrically analysis, Fourier transform infrared analysis, X-ray photoelectron spectroscopy, Field-emission scanning electron microscopy, energy dispersive spectrometry, and vibrating sample magnetometer techniques to reveal the presence of hybrid particles in the composite matrix and the existence of iron oxide and copper oxide phases. The effects of many parameters, including the initial concentrations of dye and hydrogen peroxide (H_2O_2), catalyst dosage, initial pH of the solution, and the effect of added electrolytes on the dye's degradation efficiency, have been researched. The findings indicated that the dye could be successfully degraded over a wide pH range within a reaction time of 90 min, corresponding to about 98.5% dye removal and 87% reduction of the initial total organic carbon. The improved hydroxyl radicals ($^{\bullet}OH$) and superoxide radicals ($^{-\bullet}O_2$) production efficiency and the ferric ions (Fe^{3+})/Ferrous ions (Fe^{2+}) redox cycle were occasioned by the visible light-assisted heterogeneous Fenton process catalyzed by the synthesized bio-templated magnetic copper oxide ($CuO/C/Fe_3O_4$) composite in the high degradation efficiency. In addition, the synthesized bio-templated magnetic copper oxide ($CuO/C/Fe_3O_4$) composite was reused consecutively five times with a loss of only 5% of their original degradation efficiency and can be recovered from the aqueous medium by the influence of a magnetic field while maintaining chemical stability.

Graphical abstract

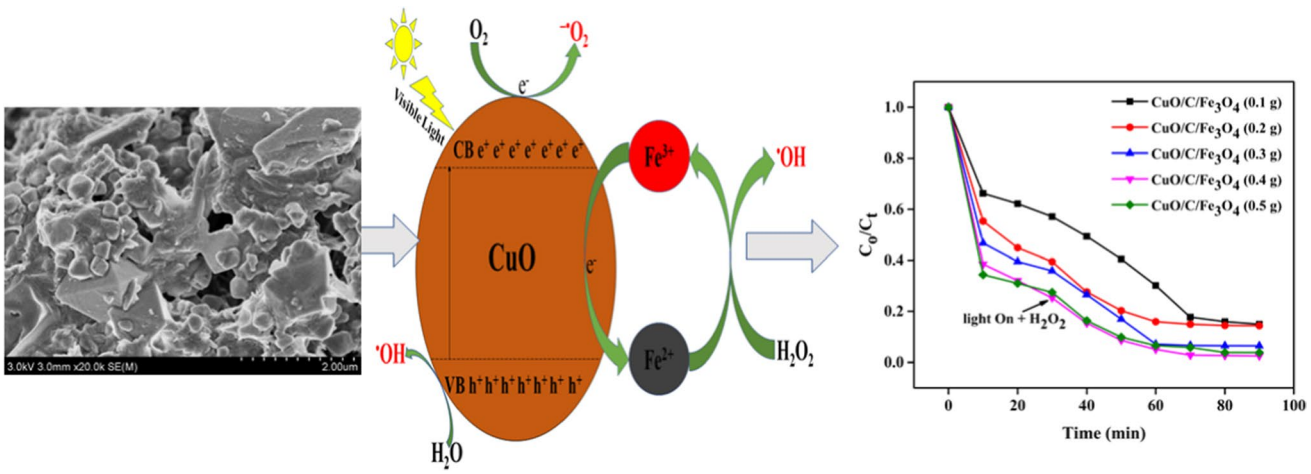

Editorial responsibility: Lifeng Yin.

Extended author information available on the last page of the article

Keywords $CuO/C/Fe_3O_4$ · Fenton-like reactions · Methylene blue dye · Polyhedral Fe_3O_4

Introduction

Vast amounts of wastewater effluents containing potentially hazardous materials such as antibiotics, dyes, pesticides, and other organic contaminants that are released from the industries have caused severe environmental concerns in recent years. Many of these pollutants are toxic and not readily biodegradable, causing harm to aquatic life as well as human health (Alani et al., 2021). Therefore, industrial wastewater containing these contaminants needs to be treated prior to discharge into bodies of water (Xu et al. 2014; Chai et al. 2016; Reza et al. 2017). Among these pollutants, Methylene Blue (MB) dye is a complex structured synthetic aromatic compound that is used to color cotton, paper, silk, leather, cosmetics, and wood (Benabbas et al. 2020; Chauhan et al. 2020). MB in water can absorb a significant amount of sunlight, preventing aquatic organisms from developing and lowering dissolved oxygen levels (Acedo-Mendoza et al. 2020). Adsorption, chemical coagulation, sedimentation, and the advanced oxidation processes (AOPs) are among the technologies being developed to eliminate these contaminants from wastewater (Chauhan et al. 2020). Among these technologies, AOPs are practical and efficient methods for degrading contaminants present in industrial wastewater. In this process, hydroxyl radicals ($^{\bullet}OH$) are generated, which accelerate and non-selectively oxidize most organic contaminants (Yao et al. 2015; Chai et al. 2016; Sharma et al. 2020). The Fenton process, among AOPs, has gotten more attention because of its excellent oxidation efficiency, accelerated oxidation kinetics, and simplicity of application (Kumar et al. 2019; Shao et al. 2020). In the Fenton process, ferrous ions (Fe^{2+}) combine with hydrogen peroxide (H_2O_2) to yield hydroxyl radicals ($^{\bullet}OH$), which in turn oxidize organic contaminants into CO_2, H_2O, and other less harmful by-products (Sum et al. 2005; Cetinkaya et al. 2018; Zhu et al. 2019). The production rate constant of ferrous ions (Fe^{2+}) via ferric ions (Fe^{3+}) reduction in the homogeneous Fenton phase has been defined as particularly slow (Shi et al. 2018; Yu et al. 2019a). Resolving the disadvantages mentioned above, UV and visible light have been used to irradiate the Fenton process, which improves the generation of Fe^{2+} from Fe^{3+} in the presence of H_2O_2 and leads to a higher yield of $^{\bullet}OH$, improving the process efficiency for removing organic contaminants from aqueous solutions (Li et al. 2017; Phan et al. 2018; Qian et al. 2018).

Numerous iron-based compounds, such as magnetite (Fe_3O_4) and ferrites, have been investigated for their effectiveness and ease of removal from the water system for the Fenton process. Magnetite is a cubic iron-containing metal oxide, with fifty percent of the Fe^{3+} occupying all tetrahedrons sites and all Fe^{2+} occupying the octahedral sites (Nguyen et al., 2017). The surface energies related to various crystallographic facets in a face-centered cubic crystal were in the range {110} > {100} > {111} (Wang 2000). In the catalytic process, the crystal with the high-energy {110} plane outperformed the crystal with the low-energy {100 or 111} plane because the high-energy plane had a higher density of low-coordinated atoms and a higher density of active surface sites (Wang 2000). To put it another way, the higher the catalyst's catalytic efficiency, the more the ratio of accessible high-energy {110} plane (Cheng et al. 2014). Most face-centered cubic crystals had exposed surfaces with {100} or {111} low-energy facets which is a typical characteristic of conventional spherical Fe_3O_4 NPs resulting in low catalytic activity. As a result, improving magnetite (Fe_3O_4) NPs' catalytic efficiency requires ramping up the number of accessible {110} surface areas. There are two main approaches for the number of accessible {110} high-energy surfaces to be increased across all the exposed surfaces in face-centered cubic crystals. One approach utilizes a mediator surface structure (examples of the mediators are oxygen, surfactants, or halides), which may selectively attach or maintain high-energy surfaces, and the other approach uses a more accurate electrochemical methodology to produce high-surface-energy metal nanocrystals (Cheng et al. 2014). Zhao et al. utilized the hydrothermal approach for the production of rhombic dodecahedral Fe_3O_4 nanocrystals. They discovered that these Fe_3O_4 nanocrystals with exposed {110} facets had greater photocatalytic performance than spherical Fe_3O_4 NPs confined by {100} facets, this they attributed to increased surface energy instead of specific surface area (Cheng et al. 2014). Guopeng et al. also synthesized polyhedral Fe_3O_4 nanoparticles with a high-energy facet of {110} via a hydrothermal method. The efficiency of degradation of polyhedral Fe_3O_4 nanoparticles catalyzed the Ultraviolet (UV)-Fenton system within 60 min of reaction was 96.7%, significantly much higher compared to spherical Fe_3O_4 NPs under the same conditions operating condition (Zhu et al. 2019). As a result, it is evident that successfully synthesizing polyhedral Fe_3O_4 NPs with high-energy {110} facets would aid in enhancing the effectiveness of important properties, including photocatalytic degradation efficiency. The acidic working pH of 3.0 and the use of high Fe content (50–80 ppm) have limited the use of polyhedral Fe_3O_4 NPs. Furthermore, considerable volumes of ferric (Fe^{3+}) hydroxide sludge is deposited after pH change when the experiment is terminated, necessitating additional handling concerns (Xu et al., 2014; Kumar et al. 2019). Additionally, the anisotropic dipolar attraction effect causes Fe_3O_4 nanoparticles to easily aggregate in an aqueous solution,

reducing their sorption ability (Zhou et al. 2017; Kumar et al. 2019). This aggregation arises from the accelerated recombination of photogenerated electrons and holes, which is a significant variable that can lower the efficiency of the photo-Fenton oxidation process (Jalaludin et al. 2015; Benabbas et al. 2020). Heterogeneous photo Fenton processes with immobilization of iron on solid catalysts can efficiently facilitate the destruction of organic pollutants at neutral or near-neutral pH, and this is advantageous compared to the homogeneous process for in situ remediations of polluted water (Tatarchuk et al. 2018; Sharma et al. 2020). Researchers have been concentrating their efforts on developing new heterogeneous Fenton-like catalysts by immobilizing Fe_3O_4 nanoparticles on different solid supports to prevent both aggregation and ease of photogenerated electrons and hole recombination effects by enhancing good catalytic efficiency and high stability. Numerous research approaches for using carbon as a support for semiconductor photocatalysts are being advanced and applied, with some researchers speculating that composite products of porous carbon materials and metal oxide photocatalysts could generate multiple active sites for catalytic degradation. (Zhao et al. 2012a; Guo et al. 2019). The performance of porous carbon loaded with magnetic metal has been studied by most researchers from different perspectives (Xiao et al. 2021). According to certain research, carbon, coupled with serving as an adsorbent or support, can operate as a sensitizer, transferring electrons to semiconducting materials and initiating the creation of powerful oxidizing radicals to boost semiconductor catalytic performance for target reactions (Gao et al. 2016a; Yu et al. 2019b). This may explain why the combination of carbon-loaded semiconductors' photocatalytic operation has been extended toward the visible region (Wang et al. 2005; Woan et al. 2009; Jiao et al. 2016; Juang et al. 2018). Among carbon supports WITH wide properties, biomass is the most extensively researched renewable carbon source. The advantages of biomass include low cost, abundant availability, and being environmentally benign (Santoso et al. 2020; Hassan and Carr 2021). Carbon, which can be obtained from biomass via hydrothermal or calcination processes, can be utilized as a substrate to allow metal particles to grow in a dispersed form on their surfaces, enhancing stability and catalytic efficiency. Carbon also acts as an adsorbent, attracting contaminants to the photocatalyst; additionally, rather than aggregating on the photocatalyst, excited electrons can be drifted away by carbon, reducing the likelihood of electrons and holes recombination and extending the lifetime of photogenerated electrons (Trogadas et al. 2014; Zhu et al. 2016). Zhai et al. used ferric citrate to synthesize magnetic ordered mesoporous carbon successfully in a "one-pot" process. The adsorption efficiency of fuchsin-based dye from an aqueous medium was significantly improved by the as-prepared magnetic-ordered mesoporous carbon composite (Zhu et al. 2016). Nailing et al. used a solvothermal method to fabricate a double conductive bio-templated magnetic bismuth oxide ($C/Fe_3O_4/Bi_2O_3$) composite using corn cob biomass as the carbon source. Because of the strong double conductivity, electrons easily migrated from Bi_2O_3 to C/Fe_3O_4, preventing the holes-electrons pairs from recombination. The double conductivity essentially stopped electrons from flowing backward to Bi_2O_3. As a result, the degrading rate of the $C/Fe_3O_4/Bi_2O_3$ composite catalyst was 91%, substantially more than either Fe_3O_4 or Bi_2O_3 (Gao et al. 2016b).

Combining Fe_3O_4 nanoparticles with visible-light active metal oxides is another technique to boost photocatalytic efficiency and extends the Fenton catalyst's effectiveness into the visible region (Douglas et al. 2016; You et al. 2019). Among the visible-light sensitive, active metal oxide, copper oxide (CuO), a p-type metal oxide having a narrow bandgap of 1.7 eV, rich earth-abundant matter, low cost, and non-toxic, has increasingly gained considerable vital attention due to its electrical, magnetic, optical, and photocatalyst characteristics (Yin et al. 2015; Sakar et al. 2016; Kshirsagar et al. 2017). When a p-type semiconductor like CuO and an n-type semiconductor like Fe_3O_4 are combined, a p-n type heterojunction is formed, decreasing photogenerated electron–hole recombination rates (Zhao et al. 2012b; Benabbas et al. 2020).

In this work, we synthesized $CuO/C/Fe_3O_4$ composite photocatalyst by a two-step procedure using pyrolysis and hydrothermal methods. Sunflower stalk was employed as the biomass carbon source on which CuO and Fe_3O_4 are templated. Methylene Blue (MB) dye was selected as the model pollutant to assess the catalyst's photon-Fenton-like activity illuminated by visible light. The ratio of CuO and Fe_3O_4 was varied to establish the optimum combination ratio that will give the best removal percent of the pollutant. The effect of the following parameters, catalyst dosage, initial dye concentration, initial pH, initial concentration of H_2O_2, and inorganic salts, on the pollutant removal percent, was also investigated. The degradation mechanism was explored to identify the principal active species liable for eliminating the pollutant.

Materials and methods

Reagents and materials

Dry sunflower stalk was collected from Changchun, China. Copper sulfate pentahydrate ($CuSO_4.5H_2O$), ferrous sulfate ($FeSO_4\bullet 7H_2O$), sodium thiosulfate pentahydrate ($Na_2S_2O_3\bullet 5H_2O$), sulfuric acid, ethanol, silver nitrate ($AgNO_3$), formic acid, p-benzoquinone (BQ), and tert-Butyl alcohol (TBA), were bought from Sinopharm Chemical Reagent Co. Ltd. Sodium hydroxide (NaOH), and Hydrogen

peroxide 30% (H_2O_2), was bought from Beijing Chemical Works. Methylene blue (MB) was purchased from Genview Scientific Inc. The chemicals were utilized without any further purification.

Catalyst synthesis and characterization

Synthesis of bio-templated copper oxide from Copper sulfate pentahydrate and sunflower stalk

Sunflower stalk (1–2 mm) was treated at 80 °C with 5% ammonium hydroxide solution for 5 h, after which it was filtered and rinsed severally with distilled water before drying for 24 h at 60 °C. After that, some predetermined quantity of the ammonium hydroxide treated Sunflower stalk was immersed in a beaker containing $CuSO_4.5H_2O$ solution (80 mM), then added NaOH solution (10 mM); the temperature was raised and maintained at 60 °C for a day. After 24 h, the sunflower stalk-loaded CuO composite was washed thoroughly utilizing distilled water, followed by finally drying at 60 °C. The dried sunflower stalk-loaded CuO composite was then calcined for 5 h at 550 °C in a tube furnace, at a heating rate of 1 °C/min in a nitrogen atmosphere to form the bio-templated Copper Oxide (CuO/C).

Synthesis of magnetite nanoparticles from ferrous sulfate and sodium thiosulfate pentahydrate

The hydrothermal method was utilized to synthesize polyhedral Fe_3O_4 NPs by introducing ferrous sulfate as a starter material (Zhu et al. 2019). Briefly described, to a jacket-glass beaker (100 mL), 2.78 g ferrous sulfate ($FeSO_4 \bullet 7H_2O$) and 2.48 g sodium thiosulfate pentahydrate ($Na_2S_2O_3 \bullet 5H_2O$) were steeped into a 30 mL distilled water, respectively, and 0.8 g sodium hydroxide was steeped into 20 mL distilled water in a 50 mL jacket-glass beaker, which was transferred to the pre-beaker and agitated for about 2 min. Subsequently, the mixture was placed into a 50 mL Teflon-lined autoclave, sealed, and heated for 12 h at 140 °C followed by cooling naturally. After that, the black precipitate was carefully rinsed and dried for 2 h in a vacuum oven at 60 °C.

Synthesis of bio-templated magnetic Copper Oxide ($CuO/C/Fe_3O_4$) by hydrothermal method

$CuO/C/Fe_3O_4$ was also synthesized utilizing the hydrothermal methodology. To a 30 mL of distilled water, 1.39 g of synthesized bio-templated Copper Oxide, 1.39 g of $FeSO_4.7H_2O$, and 1.24 g of $NaSO_4.5H_2O$ were dissolved. The mixture was stirred for 10 min, followed by adding 0.4 g of NaOH solution in drops with vigorous magnetic stirring. After that, the mixture was agitated for another 5 min before placing it in a Teflon-lined autoclave (50 mL). The Teflon-line autoclave was then sealed, and the temperature was raised to 140 °C for 12 h and cooled naturally to 24 oC. The resultant residue **bio-templated magnetic Copper Oxide** ($CuO/C/Fe_3O_4$) was rinsed with distilled water followed by drying at 60 °C in a vacuum. The synthesized bio-templated CuO and Fe_3O_4 ratios were varied in the catalyst in the ratio of 1:1, 2:1, 1:2, and 1:3, respectively.

Catalyst characterization

The crystalline phases of all the synthesized powder were studied using X-ray diffraction analysis (XRD), which was measured using a Rigaku D/Max 2550 diffractometer (Rigaku Corporation, Japan) with a Cu-kα radiation source (k = 1.54056) at 10° min^{-1} scan rate. In the range of 4000-400 cm^{-1}, Fourier Transforms Infrared Analysis (FTIR) (Nexus 670, Nicolet, USA) was utilized to identify functional groups. The samples were Thermally Gravimetrically Analyzed (TGA) using an SDT Q600 thermal gravimetric analyzer (TA Instruments, USA) ranging from 24 oC to 800 °C at a 10 °C min^{-1} ramping rate under air. The synthesized powder composite's elemental analysis was done by X-ray photoelectron spectroscopy (XPS, ESCA LAB 220-XL, Al Kα radiation). The synthesized powder morphology and the elemental compositions were analyzed on the XL-30 ESEM FEG scanning electron microscope, SEM, and Energy Dispersive Spectrometry (EDS). At room temperature, the magnetic characteristics of the composites were examined utilizing the Lakeshore 735 Vibrating Sample Magnetometer (VSM).

Photocatalytic activity measurement

The degrading of the aqueous MB solution with the addition of Hydrogen peroxide (H_2O_2) illuminated by visible light was used to assess the photo-Fenton catalytic effectiveness of the prepared $CuO/C/Fe_3O_4$ composite. To achieve the adsorption–desorption equilibrium, 100 mL of 50 mg/L MB solution was mixed with 0.1 g of catalyst and agitated in the dark for 30 min. The degrading reaction was started by adding 15 mM of H_2O_2 (30 wt %) aqueous solution under the illumination of visible light (100 W Xenon lamp was utilized as the illumination source, wavelength (λ) = 420 nm). 3 mL aliquots were collected at regular intervals and filtered promptly with 0.45 µm membrane filters. Using a UV–Vis spectrophotometer (SOPTOP 757), the concentration of residue MB was determined by analyzing the residue at 665 nm. After the reaction, the catalyst was retrieved by applying an external magnetic bar. The experiments were carried out three times, and the mean values with standard deviation were presented. Five consecutive cycles of the experiments

were performed to assess the photocatalyst's stability and recyclability, with each cycle spanning 90 min. The calculation to determine the degrading percentage of MB from the aqueous solution was done using Eq. (1) in each process.

$$\text{The percentage removal of MB}(\%) = \frac{Co - Ct}{Co} X100 \quad (1)$$

Co and Ct were the initial MB concentration at time t = 0 and at time t, respectively.

Results and discussion

X-ray diffraction analysis (XRD)

The crystal phases of the prepared CuO, Fe_3O_4, and CuO/C/Fe_3O_4 were studied utilizing X-ray diffraction analysis. As revealed in Fig. 1 (a). the diffraction peaks of Fe_3O_4 was indexed at 2θ = 30.1 (220), 35.5 (311), 43.1 (400), 53.2 (422), 57.0 (511), and 62 (440) corresponding to Joint Committee on Powder Diffraction (JCPDS) card number (JCPDS No. 75—0033) (Ghasemi et al. 2020). According to XRD peak area calculations, the percentage of the {110} facets in a single polyhedral Fe_3O_4 NPs crystal was around 37.7%, which was consistent with what modeling predicted. The CuO/C/Fe_3O_4 XRD patterns with varied CuO and Fe_3O_4 compositions include not only the distinctive Fe_3O_4 diffraction peaks but also the typical peaks of monoclinic CuO (JCPDS No. 75—1517) Fig. 1. (b.) The CuO/C/Fe_3O_4 peak at 35.5° was correlated to both the CuO phase's (-111) plane and the Fe_3O_4 phase's (311) plane (Fig. 1. (b), indicating the presence of CuO/C/Fe_3O_4 heterojunctions (Tian et al. 2016). However, the presence of porous bio-templated CuO in the composite enhances the sensitivity of the modified Fe_3O_4 NPs in the visible light region.

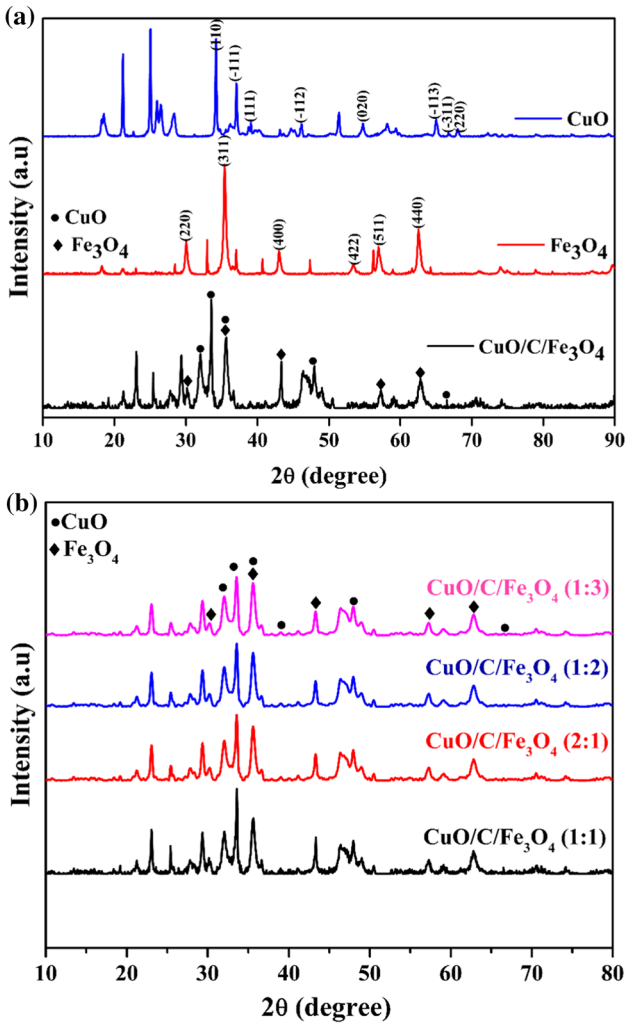

Fig. 1 XRD patterns of CuO, CuO/C, Fe_3O_4, and CuO/C/Fe_3O_4 (**a**) XRD patterns of CuO/C/ Fe_3O_4 with varying compositions of CuO/ Fe_3O_4 molar ratios (**b**)

Fourier transforms infrared (FTIR) analysis

Figure 2 depicts the FTIR spectra of Fe_3O_4, CuO/C, and CuO/C/Fe_3O_4. The FTIR spectrum of Fe_3O_4 nanoparticles contains three main peaks of significance: 585, 1637, and 3413.73 cm^{-1}, which correspond to Fe–O bonds in the crystal lattice of Fe_3O_4 C-H bonds, and O–H bonds, respectively. The presence of the C-H and O–H bonds is most likely due to the usage of water and ethanol during synthesis; this finding was confirmed and published (Yang et al. 2010; Takai et al. 2019). CuO/C displays a sharp band at roughly 681 cm^{-1}, traceable to the Cu–O stretching mode, and 1619 cm^{-1}, which is associated with the C-H band, indicating that carbon is present as the organic framework supporting the CuO nanoparticles. The CuO/C lattice stretching water molecules cause broadband at 3313.31 cm^{-1} in the CuO/C framework. The major bands of 581, 675, 1631, and

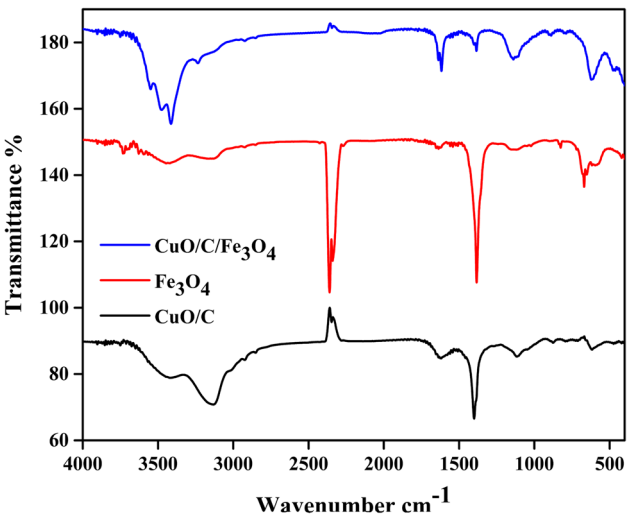

Fig. 2 Infrared spectra of CuO/C, Fe_3O_4, and CuO/C/Fe_3O_4

3500–3100 cm^{-1} in the spectrum of CuO/C/Fe_3O_4 correspond to Fe–O of Fe_3O_4, Cu–O of CuO, C-H of CuO organic framework, and O–H of inherent and adsorbed water molecules, respectively. Therefore, the preparation of CuO/C/Fe_3O_4 nanoparticles is also confirmed by the FTIR study.

Thermogravimetric analysis (TGA)

TGA was utilized to assess the carbon content of the CuO/C/Fe_3O_4 composite. To estimate the carbon content in CuO/C/Fe_3O_4, a thermogravimetric analysis was performed in the air. The loss of absorbed water is connected to the weight loss between 100 °C and 280 °C, as shown in Fig. 3. The oxidation of both CuO and Fe_3O_4 causes weight gain from 280 to 335 °C; prior researchers also saw and documented this phenomenon (Chai et al. 2016; Li et al. 2017). The oxidation of carbon could be responsible for the weight loss after 335 °C, indicating that carbon is present in the catalyst matrix (Sun et al. 2017).

X-ray photoelectron spectroscopy (XPS) analysis

The elemental composition, chemical, and electronic states of the atoms within CuO/C, Fe3O4, and CuO/C/Fe3O4 were measured using X-ray Photoelectron Spectroscopy (XPS) to investigate the catalyst surface chemistry. The survey scans spectral of CuO/C, Fe_3O_4, and CuO/C/Fe_3O_4 are predominantly made of Fe, O, C, and Cu, respectively, owing to the charge state of elements presents in Fig. 4a. The existence of three major elements, Fe, Cu, and O, and an increase in the intensity of the oxygen peak, were seen in the CuO/C/Fe_3O_4 heterojunction, indicating that CuO/C/Fe_3O_4 was synthesized. The main elements present in the CuO/C/Fe_3O_4 photocatalyst are shown in the deconvoluted spectrum (Fig. 4 (b-d)). Figure 4(b) shows the deconvolution of the Cu 2p XPS spectra into four binding energies: 933.5, 942, 953.6, and 962.2 eV. Cu $2p_{3/2}$ and Cu $2p_{1/2}$ have high-resolution peaks at 933.5 and 953.6 eV, respectively, indicating that Cu in the produced CuO/C/Fe_3O_4 photocatalyst is in the oxidation state Cu^{2+} (Taylor-Pashow et al. 2009; Sharma et al. 2020). Two satellite peaks at 942 and 9622.2 eV, attributable to the d^9 configuration of Cu^{2+}, were also found, attesting to the existence of CuO; this result aligned with previously reported findings (Sun et al. 2018; Uthirakumar et al. 2020). Figure 4c depicts a typical Fe 2p spectra with two prominent peaks at 711.2 and 724.5 eV, corresponding to Fe $2p_{3/2}$ and Fe $2p_{1/2}$ spin–orbit split doublets, respectively; the findings are in agreement with previous research. (Xu et al. 2014; Li et al. 2017). Furthermore, the binding energy of lattice and adsorbed oxygen elements is represented by the XPS deconvoluted spectra of O1s with peaks at 533.3, 531.1, and 530.4 eV Fig. 4 (d) (Li et al. 2017; Sun et al. 2018; Uthirakumar et al. 2020). Furthermore, there was a redshift in binding energy compared to Cu 2p (Fig. 4b) in their pure and composite forms, beneficial for light excitation. The redshift movement was also observed in the Fe 2p Fig. 4c.

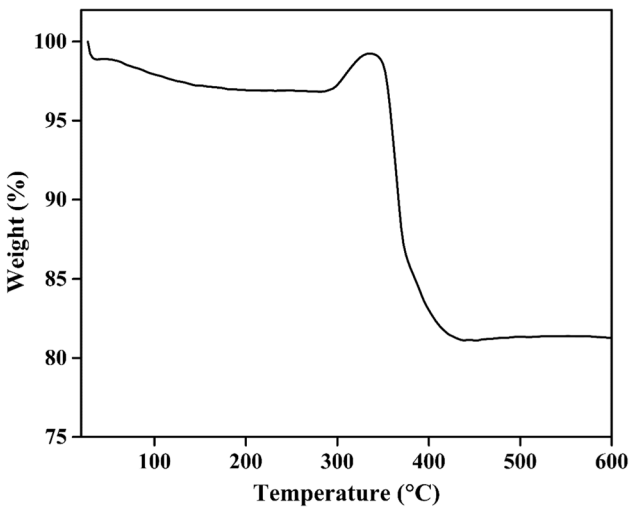

Fig. 3 Thermogravimetric curve of CuO/C/Fe3O4

field-emission scanning electron microscopy (FE-SEM) analysis

The synthesized CuO/C/Fe_3O_4 composites were examined by the FE-SEM to investigate their morphology. Figure 5a reveals that the CuO particles are compacted packed, similar to the particles of Fe_3O_4 (Fig. 5b), while in the CuO/C/Fe_3O_4 composite (Fig. 5c), the structure has been loosened up because of the hierarchical porous microstructure due to the presence of the sunflower stalk. Figure 5c shows that after the template was removed, the CuO/C/Fe_3O_4 sample maintained the sunflower stalk nest's initial hierarchical porous microstructure. This porous architecture improves particle interconnection, minimizes photo-induced hole/electron recombination, and boosts the adsorption of MB molecules. The Energy Dispersive Spectrometry (EDS) analysis was also used to confirm the synthesized catalyst's elemental compositions. Cu, Fe, C, and O are the predominant atoms of CuO/C/Fe_3O_4, with weight percentages of 11.68 percent, 19.51 percent, 42.24 percent, and 23.03 percent, respectively, as seen in Fig. 5d.

Magnetism study

Vibrating Sample Magnetometer (VSM) was utilized to study the hysteresis loops of Fe_3O_4 and CuO/C/Fe_3O_4 at 300 K, Fig. 6. The saturation magnetization (Ms) value of the pure polyhedral Fe_3O_4 is ca. 49.2 emu/g, while the CuO/C/Fe_3O_4 composite is ca. 34.2 emu/g, indicating the CuO/C/Fe_3O_4 composite is superparamagnetic. The

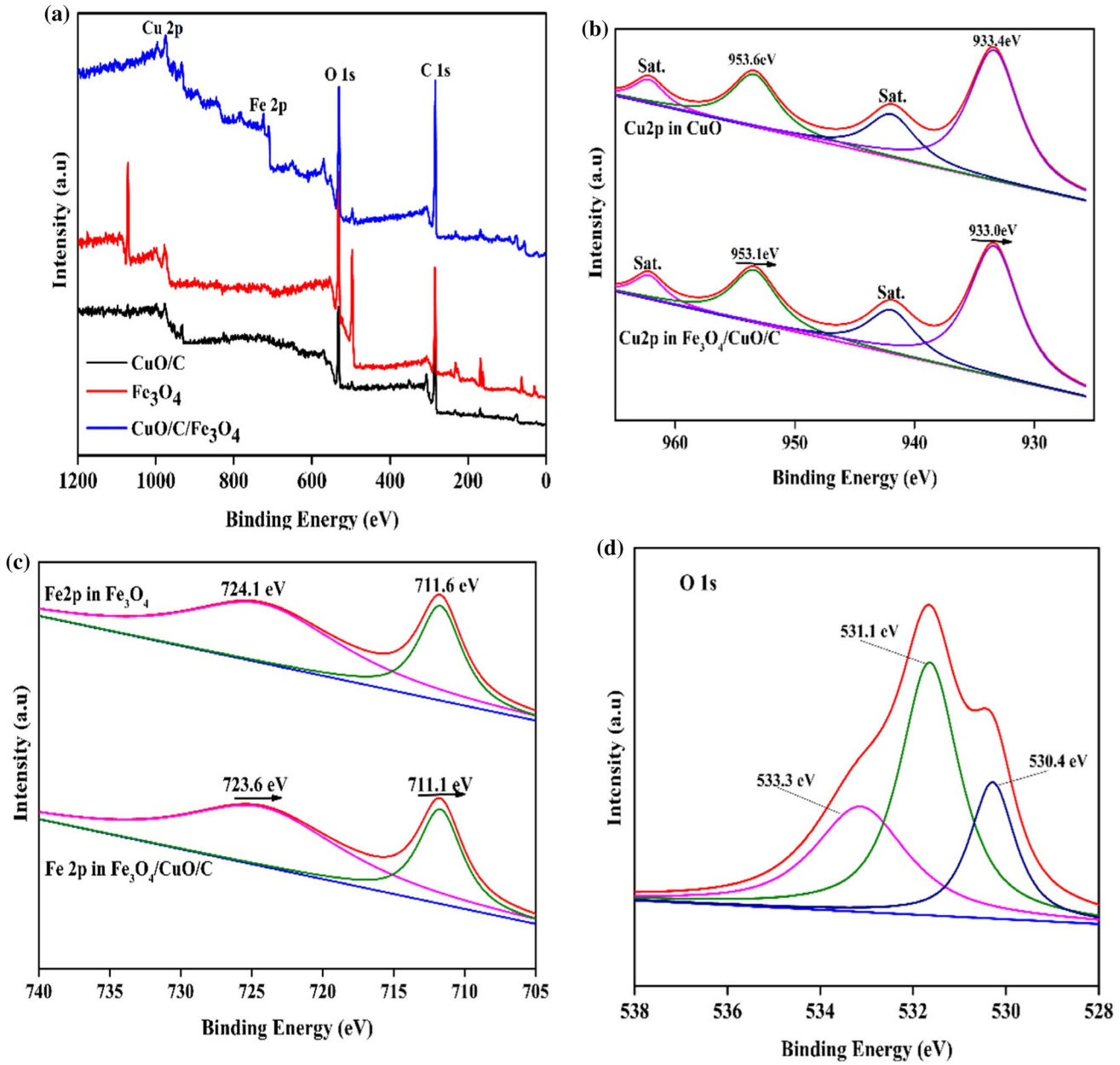

Fig. 4 X-ray photoelectron spectroscopy (XPS) wide scan of CuO/C, Fe_3O_4, and CuO/C/Fe_3O_4 (**a**), high-resolution spectra of Cu 2p state (**b**), Fe 2p state (**c**), (**b**–**d**), and O 1 s state (**d**)

inclusion of doped non-magnetic CuO and C could explain the decline in the magnetic property (Feng et al. 2017; Yu et al. 2018). CuO/C/Fe_3O_4 may be re-dispersed with ease for reuse, as shown in the Fig. 6 insert, after separating and manipulations with an externally applied magnetic bar. As a result, the separation, recovery, and reuse of CuO/C/Fe_3O_4 photocatalyst may be aided.

Photocatalytic activity

The photocatalytic effectiveness of the various catalyst systems on the rate of degradation of (Methylene Blue) MB is depicted in Fig. 7a. When illuminated with visible light only, MB is stable, and no noticeable decline in its concentration was observed (that is, no photolysis of MB was seen) after

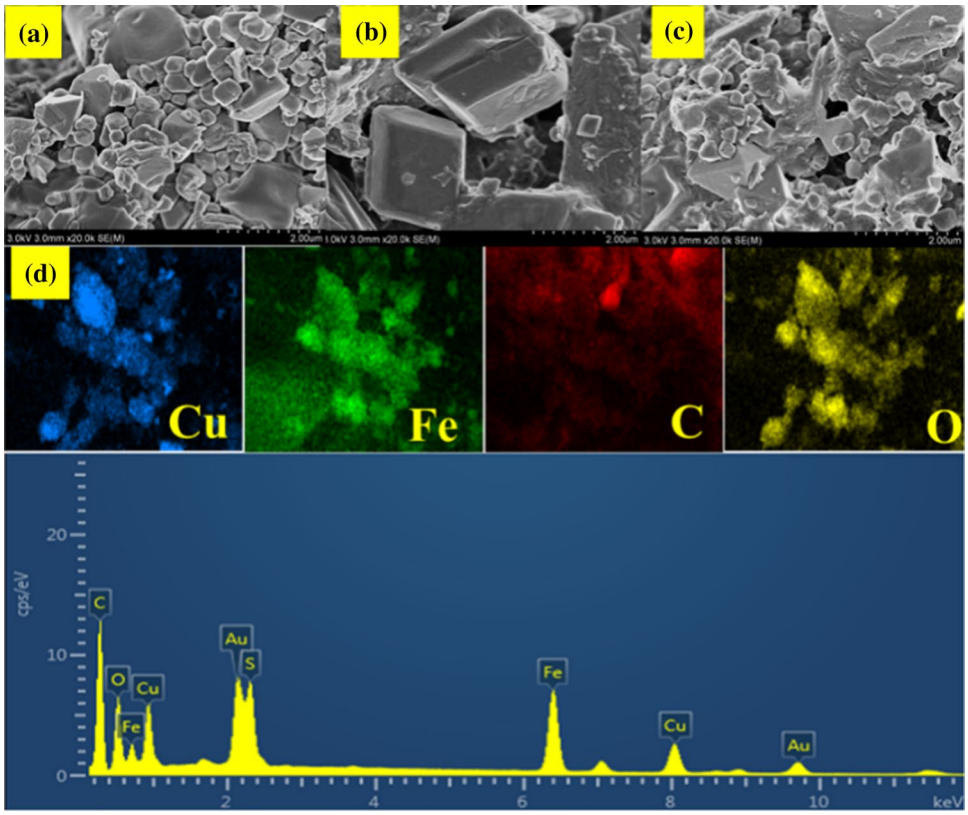

Fig. 5 SEM image of CuO (**a**) Fe_3O_4 (**b**) CuO/C/Fe_3O_4 (**c**) and EDS Elemental mapping (**d**)

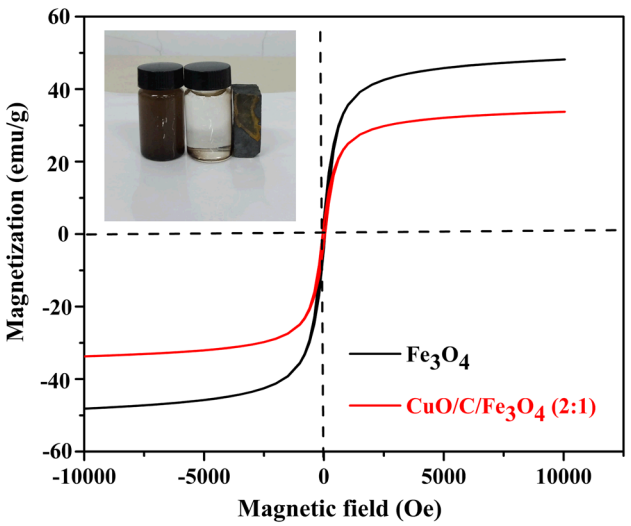

Fig. 6 Magnetic hysteresis loops of Fe_3O_4 and CuO/C/Fe_3O_4 (1:1) NPs at 300 K

90 min under visible light illumination without employing a suitable catalyst Fig. 7a. While in the H_2O_2-visible light system, 37% MB elimination was achieved due to H_2O_2 photolysis caused by visible light irradiation (H_2O_2 + visible light → $^{\bullet}OH + OH^-$). Photocatalytic degradation of MB with CuO/C/Fe_3O_4 as catalyst achieved a 45.9% MB removal. In the photo-Fenton process using polyhedra Fe_3O_4 as catalyst ($Fe_3O_4 + H_2O_2$ + visible light), 52.9% MB was removed, while in the heterogeneous photo-Fenton process (CuO/C/$Fe_3O_4 + H_2O_2$ + visible light), 85.1%, MB was removed within 90 min Fig. 7a. The results show that MB is successfully degraded under visible light irradiation by using CuO/C/Fe_3O_4 as catalysts and H_2O_2 as an aid.

The influence of Fe_3O_4 and CuO molar ratio on Methylene Blue dye degradation

The influence of CuO/Fe_3O_4 molar ratio on the photo-Fenton catalytic activities of the prepared CuO/C/Fe_3O_4 composites for removal of MB was researched, and the findings are displayed in Fig. 7b. The photo-Fenton catalytic activities of CuO/C/Fe_3O_4 (1:1), CuO/C/Fe_3O_4 (1:2), CuO/C/Fe_3O_4 (2:1), and CuO/C/Fe_3O_4 (1:3) achieved a removal rate of 76.1%, 73.9%, 85.1% and 72.1% respectively. From the results presented in Fig. 7b, CuO/C/Fe_3O_4 (2:1) composites achieved the highest removal rate compared to other molar ratios of CuO/Fe_3O_4, suggesting that CuO played a salient role in the removal of MB by the heterogeneous photo-Fenton process. Furthermore, the significantly higher activity of CuO/C/Fe_3O_4 (2:1) molar ratio as compared to the other molar ratios was due to adequacy in the proportion of its heterojunctions. Due to the lower proportion of heterojunctions in CuO/C/Fe_3O_4 (1:1), CuO/C/Fe_3O_4 (1:2), and CuO/C/Fe_3O_4 (1:3), their activities are lower. This result

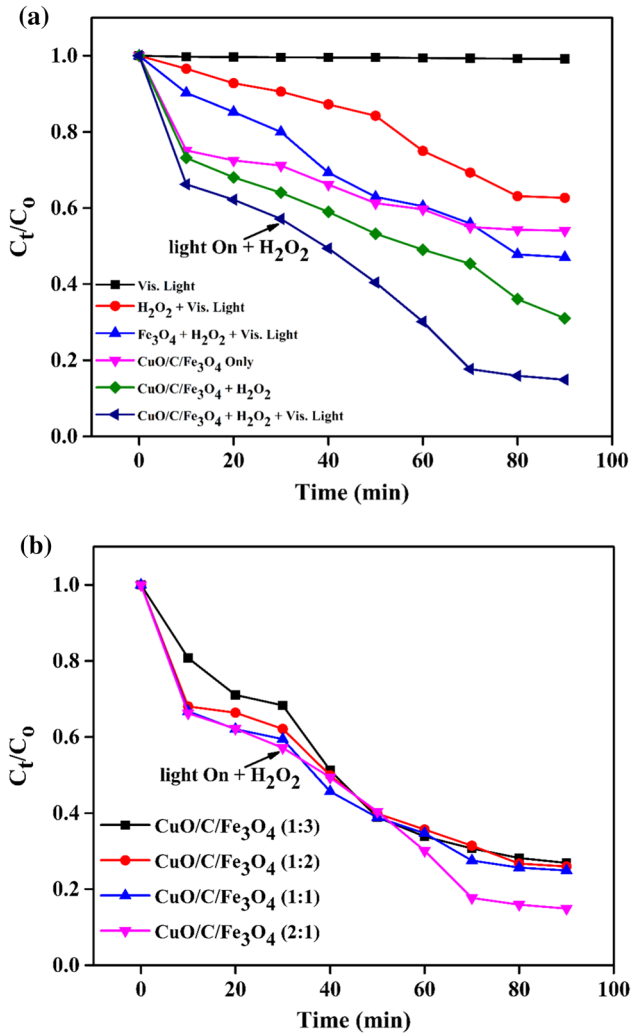

Fig. 7 Removal of MB under different conditions (**a**), different catalyst compositions (**b**). Reaction parameters: Except for the investigated parameters, MB concentration = 50 mg/L, catalyst dosage = 0.1 g/L, H_2O_2 = 15 mM, pH = 7.0, time 90 min and temperature 24 °C

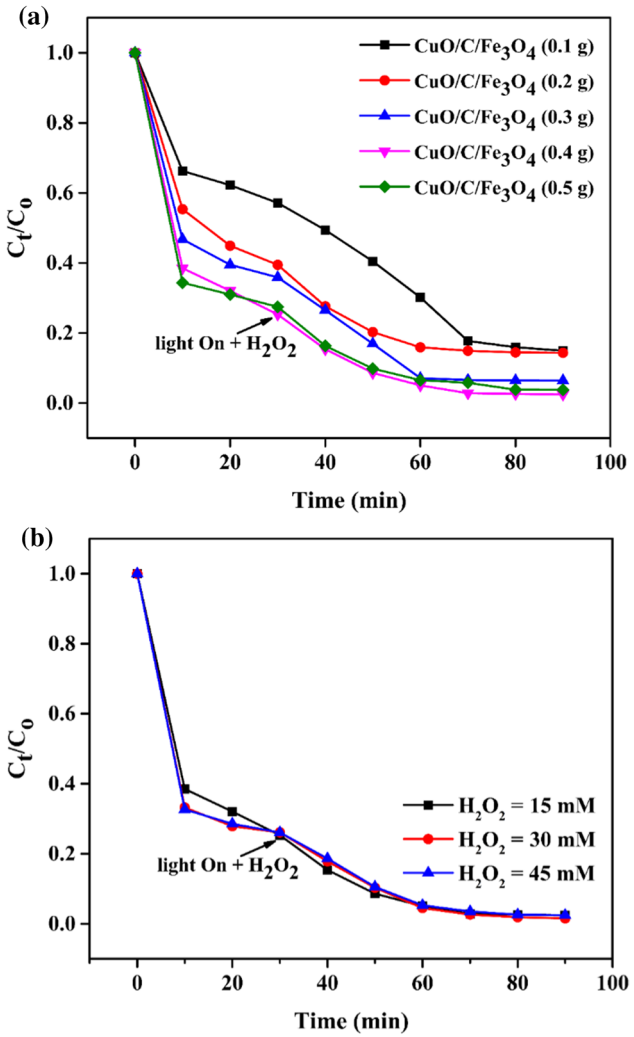

Fig. 8 Effect of Catalyst dosage on MB removal (**a**), the effect of initial concentration of H_2O_2 (**b**). Reaction parameters: Except for the investigated parameters, MB concentration = 50 mg/L, catalyst dosage = 0.4 g/L, H_2O_2 = 15 mM, pH = 7.0, time 90 min and temperature 24 °C

also emphasizes the significance of heterostructures, which serve as charge migration interfaces. Due to the higher performance of the CuO/C/Fe_3O_4 (2:1), it was adopted for further processes.

Effect of catalyst dosage on Methylene Blue dye degradation

The impact of the catalyst dosage was researched for the heterogeneous photo-Fenton process, and the findings are shown in Fig. 8a. For catalyst dosages of 0.1, 0.2, 0.3, 0.4 and 0.5 g the MB removal rates are 85.1, 88.7, 92.6, 98.5, and 95.2% respectively. As catalyst dosages increased from 0.1 – 0.4 g, the dye's removal rate was found to increase. Because increasing catalyst dosage generates increased radical species production, the increase in accessible active catalytic sites on the photocatalyst surface resulted in a higher MB removal rate. When the dosage was increased to 0.5 g, the catalytic performance of the system was retarded (Fig. 8a). As the catalyst dosage is increased, the efficiency of the photo-Fenton system decreases. Excess photocatalyst clumped together and acted as a visible light screen. Another explanation for the lower removal rate is that increasing the catalyst loading increases the cloudiness of the solution, which reduces photon flux penetration in the reactor and hence lowers the photocatalytic degradation rate (Lucas and Peres 2007; Divya et al. 2013; Reza et al. 2017). As a result, at 0.4 g photocatalyst dosage was the photocatalytic system's performance peaks.

Effect of the initial concentration of H_2O_2 on Methylene Blue dye degradation

The determination of the impact of H_2O_2 addition on MB removal, varying concentrations of H_2O_2 ranging from 15 – 45 mM were applied to an aqueous solution of MB at a specific pH (pH = 7) in the presence of 0.4 g of CuO/C/Fe_3O_4 (2:1) composite. From the results obtained in Fig. 8b, the elimination rate of MB increases when the initial concentration of H_2O_2 is increased from 15 – 30 mM. The improvement in the rate of MB elimination was attributed to an improvement in the creation of hydroxyl radicals (•OH), which are created when H_2O_2 interacts with Fe^{2+} to produce •OH radicals, which rapidly destroy the MB molecule. However, increasing the H_2O_2 concentration to 45 mM resulted in a lower MB removal rate. At a higher H_2O_2 concentration, H_2O_2 serves as a scavenger for hydroxyl radicals, resulting in the creation of peroxyl radicals (HOO•), which are less reactive than •OH radicals and have a reduced oxidative effect. (Maia et al. 2014). The generated $HO_2^{\bullet}$ competes with •OH to eliminate the MB dye chromophore and causes a reduction in the degradation percent of MB (Coleman et al. 2007). As a result, increasing the H_2O_2 concentration above the optimum concentration reduced the MB degradation efficiency of the reaction. The optimum H_2O_2 concentration in this research is 30 mM.

Effect of initial pH on Methylene Blue dye degradation

In the Fenton reaction, the initial pH of the aqueous solution has been reported as an essential factor affecting the rate of elimination of recalcitrant contaminants (Wu et al. 2021). As a result, while keeping other parameters constant, it is necessary to evaluate the impact of pH on MB deterioration in the heterogeneous photo-Fenton process. The impact of solution pH on MB degradation was researched by varying the initial pH values ranging from 3 to 9, Fig. 9a. The photodegradation efficiency of MB in the photo-Fenton process using the as-prepared CuO/C/Fe_3O_4 composite as catalyst had no significant effect on changing initial pH, as demonstrated by the findings in Fig. 9a, suggesting that the prepared CuO/C/Fe_3O_4 composite could be utilized through a wide pH range.

Effect of the initial concentration of Methylene Blue rate of Degradation

The impacts of the MB's initial concentration on photodegradation performance were presented in Fig. 9b. As the initial MB concentration varied from 50 to 150 mg/L, the percentage of MB removal from aqueous solution gradually decreased from 98.5 to 94.4% in 90 min. The decrease in efficiency of MB removal can be due to some of these

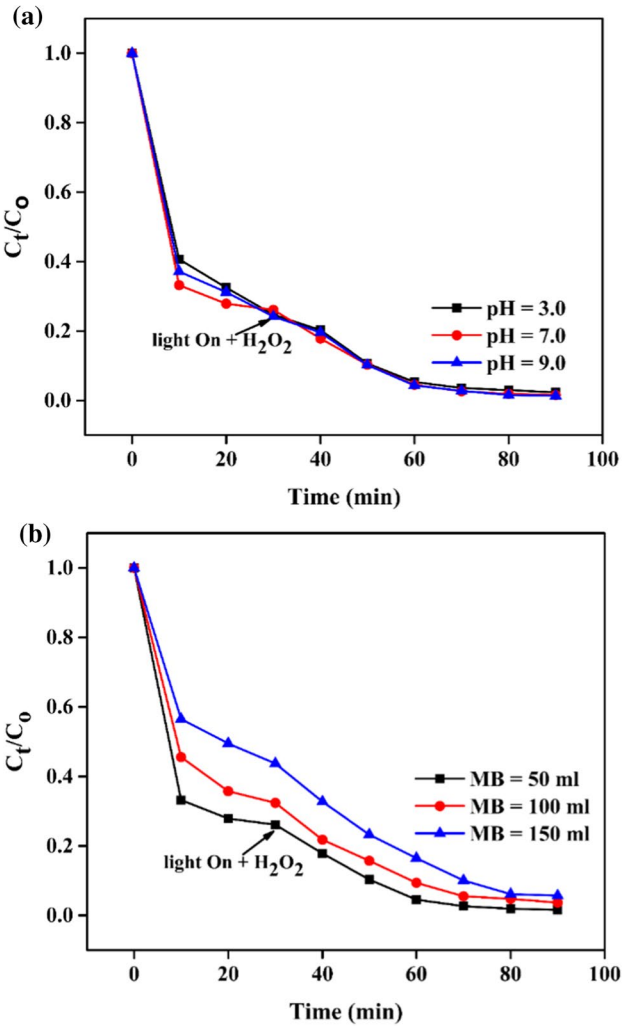

Fig. 9 Effect of initial pH (**a**), initial concentration of MB (**b**) Reaction parameters: Except for the investigated parameters, MB concentration = 50 mg/L, catalyst dosage = 0.4 g/L, H_2O_2 = 30 mM, pH = 7.0, time 90 min and temperature 24 °C

reasons: firstly, as the initial MB concentration increases, so does the amounts of dye molecules accessible for adsorption onto the CuO/C/Fe_3O_4 surface. The yield of •OH radicals in the aqueous solution remained constant under the same operating conditions. The amount of •OH used was insufficient to decompose the MB's high initial concentration, resulting in a decline in removal efficiency. Furthermore, the larger MB molecules on the photocatalyst may have consumed a more significant number of active sites. That is to say, with higher MB concentrations, fewer active sites became accessible for the breakdown of H_2O_2, resulting in a reduced rate of •OH production (Es'haghzade et al. 2017). Second, when the initial concentration of MB increases, the solution's cloudiness also increases, making Visible light radiation unable to reach the aqueous solution of MB dye and hindering the photocatalyst's capacity to use the light (Cong and Xu 2011).

Effect of inorganics anion on the degradation rate of Methylene Blue

Inorganic anion commonly coexists with organic contaminants in wastewater and can affect wastewater treatment's photodegradation efficiency. The influences of these anions such as Cl^-, SO_4^{2-}, NO_3^-, and HCO_3^-, usually present in wastewater, tend to compete with the pollutants to consume reactive radicals during the Fenton oxidation process. The results are shown in Fig. 10 (a) indicated that these anions inhibited the efficiency with which MB could be removed from an aqueous solution. The ability of anions to act as hydroxyl radical scavengers is undoubtedly responsible for this inhibition; prior studies have confirmed similar findings (Legrini et al. 1993). These ions have the potential to deactivate photocatalysts by blocking active sites on the surface of $CuO/C/Fe_3O_4$. Even though the produced radical anions, $Cl^{\bullet-}$, $SO_4^{\bullet-}$, $NO_3^{\bullet-}$, and $CO_3^{\bullet-}$, are oxidants, their oxidation powers are lower compared to those of the hydroxyl radicals, which conforms to previous reports of some previous researchers (Hasmath Farzana and Meenakshi 2014). Anions like sulfate, chloride, bicarbonate, and nitrate have also been observed to react with positive h^+/$^{\bullet}OH$, resulting in their respective ionic radicals, which are less reactive than $^{\bullet}OH$; this observation is consistent with earlier research findings (Zhu et al. 2011). As a result, these inorganic entities have a deleterious impact on the Fenton oxidation process to eliminate MB.

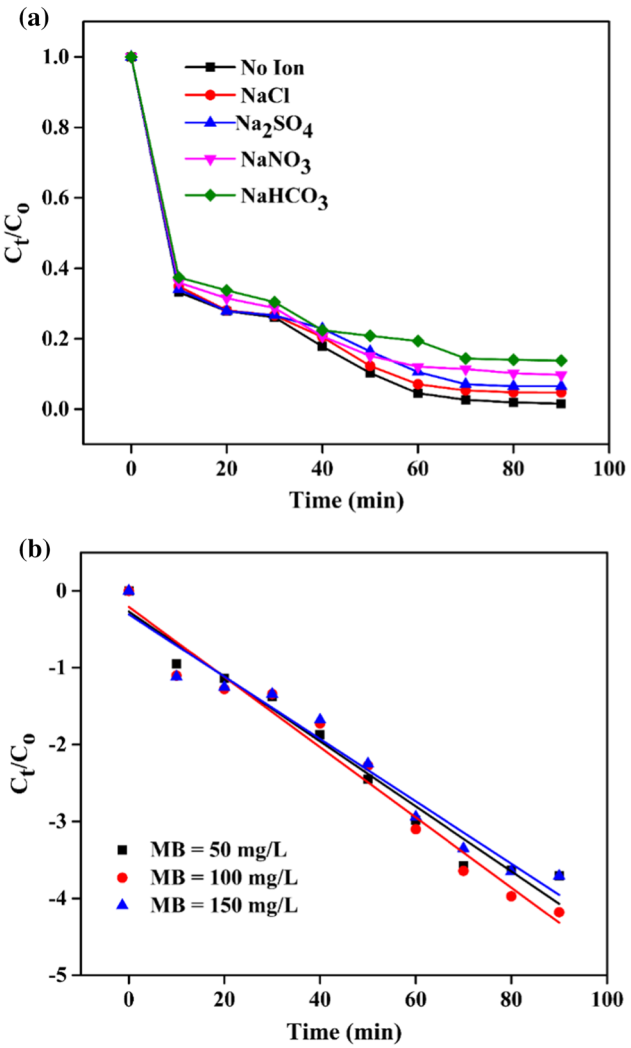

Fig. 10 Effect of Inorganics species (**a**) and plot of ln (C_t/C_o) against time (**b**) Reaction parameters: Except for the investigated parameters, MB concentration = 50 mg/L, catalyst mass = 0.4 g/L, H_2O_2 = 30 mM, pH = 7.0, time 90 min and temperature 24 °C

Kinetic study on the degradation rate of Methylene Blue

The findings of a kinetic investigation on various initial concentrations of MB are shown in Fig. 10 (b) and Table 1, while a comparison of catalytic activities of different composites is presented in Table 2. The apparent rate constants are determined from plots of ln (C_t/C_o) vs. irradiation time. With respect to the irradiation time, the photo-Fenton degradation processes of the MBs followed a pseudo-first-order kinetic model Eq. (2).

$$\ln\left(\frac{Ct}{Co}\right) = -kt \tag{2}$$

where Co (mg/L) is the initial MB concentration, C_t (mg/L) is the MB concentration at time t, and k is the rate constant ($\min -^1$).

Mechanism of MB degradation by the photo-Fenton-like reaction

A series of radical scavengers were utilized for the determination of the main reactive species in the photodegradation of MB. The scavengers employed are Tert-Butyl Alcohol (TBA) for hydroxyl radicals $^{\bullet}OH$, p-benzoquinone (BQ) for superoxide radical $^{-\bullet}O_2$ (Yao et al. 2015), silver nitrates ($AgNO_3$) for photogenerated electrons (e^-), and formic acid for photogenerated holes (h^+) (Feng et al. 2017). From the result obtained in Fig. 11a, there was a suppression of the photo-Fenton MB degradation in the order of addition of the

Table 1 Rate Constants values for Methylene Blue degradation at different concentration

Concentration of MB (mg/L)	50	100	150
Rate Constant k (min^{-1})	0.26816	0.20671	0.30433
Initial reaction rate (mgL^{-1} min^{-1})	0.04225	0.04568	0.04056
Adjacent R-Square (R^2)	0.96507	0.96393	0.95730

Table 2 Comparison of catalytic activities of different composites for degradation of MB

Catalyst	Operational condition	Catalytic performance	Reference
$CuO/C/Fe_3O_4$	Catalyst (0.4 g/L); dye conc. (50 mg/L); H_2O_2 (30 mM); time (90 min); Visible light	98.5%	This work
$Fe_3O_4/C/Cu_2O$	Catalyst (0.5 g/L); Dye conc. (100 mg/L); H_2O_2 (163.7 mM); time (60 min); Visible light	97.2%	(Chai et al. 2016)
Fe_3O_4@C/Cu	Catalyst (0.5 g/L); Dye conc. (100); H_2O_2 (0.5 ml); time (140 min); Visible light	99.6%	(Zhang et al. 2014)
Fe_3O_4-CuO@C(C-R)	Catalyst (0. 1 g/L); Dye conc. (10 mg/L); H_2O_2 (19.8 mM); time (120 min); visible light	97.7%	(Qin et al. 2020)
Fe_3O_4/CuO	Catalyst (0.05 g/L); Dye conc. (10 mg/L); H_2O_2 (32 mmol/L); time (120 min); visible light	95%	(Ghasemi et al. 2020)

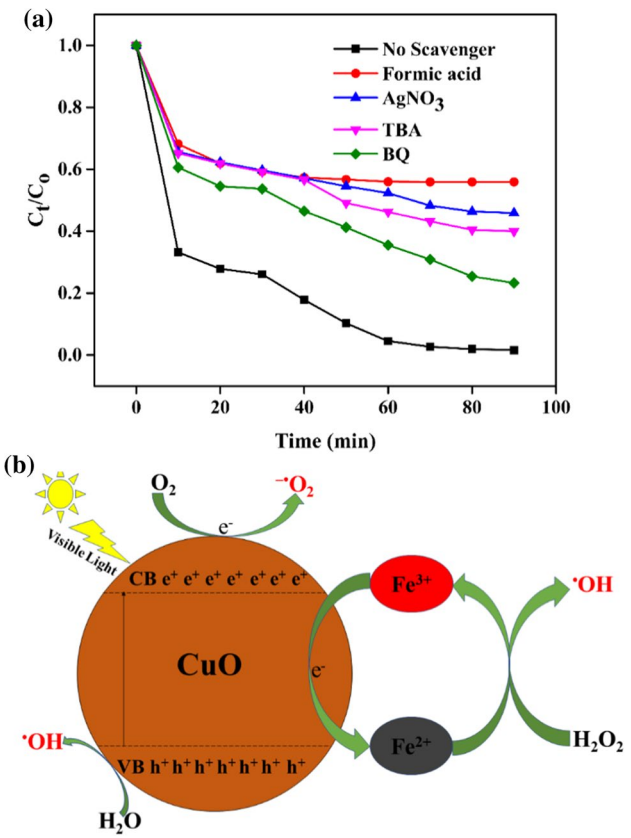

Fig. 11 Effects of scavengers on the photodegradation of MB by $CuO/C/Fe_3O_4$ (2:1)/H_2O_2/visible light irradiation system (**a**) and Schematic depiction of the photo-Fenton-like mechanism for MB degradation under Visible light illumination in the presence of $CuO/C/Fe_3O_4$ composites (**b**). Reaction parameters: Except for the investigated parameters, MB concentration = 50 mg/L, catalyst mass = 0.4 g/L, H_2O_2 = 30 mM, pH = 7.0, time 90 min and temperature 24 °C

following scavengers: formic acid > $AgNO_3$ > TBA > BQ, respectively. The result indicated that all radicals are generated during the degradation process and responsible for the photo-Fenton MB degradation in the following order: $h^+ > e^- > {}^{\bullet}OH > {}^{-\bullet}O_2$.

The plausible explanation for the mechanism of photodegradation of MB using $CuO/C/Fe_3O_4$ as the catalyst is as follows (Eqs. 3–8). When visible light is irradiated on the as-prepared $CuO/C/Fe_3O_4$ catalyst surface, photogenerated electrons and holes are excited from its surface (Eq. 3). Subsequently, the excited electrons catalyze the decomposition of O_2 into ${}^{-\bullet}O_2$ (Eq. 4). The excited holes catalyze the decomposition of the adsorbed water (H_2O) to produce ${}^{\bullet}OH$ (Eq. 7). Photogenerated electrons from the as-prepared catalyst surface enhance the Fe^{3+}/Fe^{2+} cycle efficiency (Eq. 6). The Fe^{3+} released during the Fenton reaction serves as an electron acceptor, preventing photogenerated hole-electron recombination, owing to the $CuO/C/Fe_3O_4$ heterostructure's well-suited interfacial interaction. The bio-template (carbon content) in the as-prepared catalyst composition provides an enriched microenvironment to adsorbs the MB molecules from the aqueous solution. As a result, it is concluded that the photodegradation of MB into CO_2 and H_2O is a synergistic effect between ${}^{\bullet}OH$ and ${}^{-\bullet}O_2$ (Eq. 8). The schematic diagram illustrating the proposed photodegradation of MB under visible light irradiation in the presence of $CuO/C/Fe_3O_4$ composites is shown in Fig. 11b.

$$CuO + hv \rightarrow h^+ + e^- \quad (3)$$

$$O_2 + e^- \rightarrow {}^{-\cdot}O_2 \quad (4)$$

$$Fe^{2+} + H_2O_2 \rightarrow Fe^{3+} + {}^{\cdot}OH + OH^- \quad (5)$$

$$Fe^{3+} + e^- \rightarrow Fe^{2+} \quad (6)$$

$$H_2O + h^+ \rightarrow {}^{\cdot}OH + H^+ \quad (7)$$

$${}^{\cdot}OH/{}^{-\cdot}O_2 + MB \rightarrow CO_2 + H_2O + \text{By products} \quad (8)$$

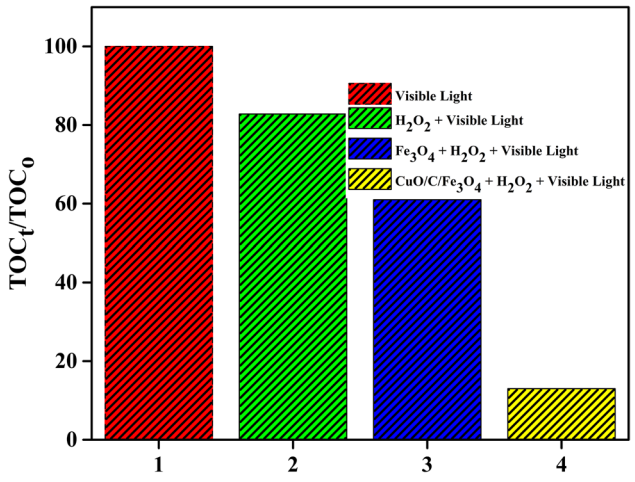

Fig. 12 Mineralization study of MB for different catalyst processes. Reaction parameters: Except for the investigated parameters, MB concentration = 50 mg/L, catalyst dosage = 0.4 g/L, H_2O_2 = 30 mM, pH = 7.0, time 90 min and temperature 24 °C

Residue Total Organic Carbon (TOC) after degradation of Methylene Blue

TOC analysis was carried out to estimate the amount of total organic carbon that remains in the aqueous solution of methylene blue dye after the photo-Fenton oxidation reaction. From the results obtained in Fig. 12, the visible light process had 98% residual TOC. The creation of •OH through the photolysis of H_2O_2 resulted in a TOC removal rate of 17.8% for visible light-H_2O_2, 39 percent for visible light-Fe_3O_4–H_2O_2, and 87 percent for CuO/C/Fe_3O_4–H_2O_2-visible light. Comparing the photo-Fenton oxidation activities of visible light-Fe_3O_4–H_2O_2 and visible light-CuO/C/Fe_3O_4–H_2O_2 for TOC removal rate, it is evident that the CuO/Fe_3O_4 interfaces heterostructure enhances the efficiency of removal of TOC similar to what was observed for the removal MB.

Reusability and chemical stability of the as-prepared CuO/C/Fe_3O_4 catalyst on the degradation of Methylene Blue dyes

The reusability of the CuO/C/Fe_3O_4 composite is a critical factor to assess before it can be adopted for practical applications. Therefore, the CuO/C/Fe_3O_4 composite was recycled under the same experimental conditions for five consecutive runs. The results in Fig. 13a indicated that the catalyst's photocatalytic performance exhibited no remarkable decline, as there was only a 5% reduction in photocatalytic performance from the first run to the fifth run. The loss of a little amount of catalyst during the cleaning procedure at the end of each run could explain the slight decline in photocatalytic effectiveness. Despite this, the CuO/C/Fe_3O_4 composite demonstrated excellent chemical stability as there was no observable difference in the XPS peaks spectral of the catalyst before and after reuse Fig. 13b.

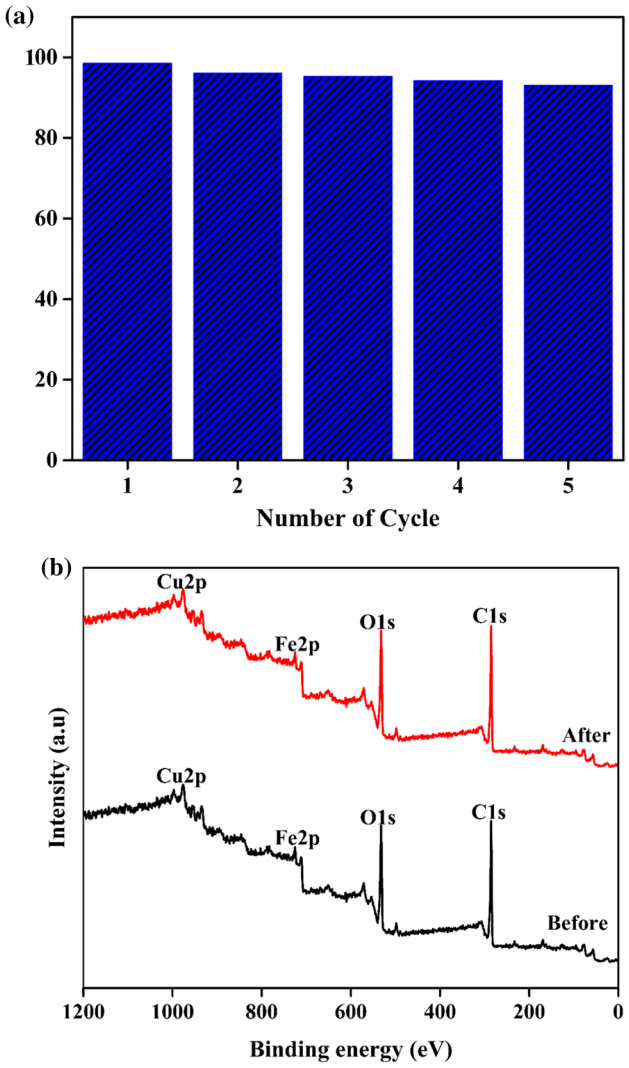

Fig. 13 CuO/C/Fe_3O_4 composite reusability for degradation of MB (**a**), XPS analysis CuO/C/Fe_3O_4 before and after reuse (**b**). Reaction parameters: Except for the investigated parameters, MB concentration = 50 mg/L, catalyst dosage = 0.4 g/L, H_2O_2 = 30 mM, pH = 7.0, time 90 min and temperature 24 °C

Conclusion

In conclusion, a simple and economical method was used to modify polyhedral Fe_3O_4 NPs with porous bio-templated copper oxide using sunflower stalk as the bio-template. A microenvironment was generated for the confinement of MB molecules by the sunflower-stalk-templated CuO skeleton, while the presence of CuO enhances the sensitivity of the synthesized catalyst towards visible light. Interfacial

contacts involving CuO and Fe_3O_4 increased the Fe^{3+}/Fe^{2+} cycle effectiveness. CuO/C/Fe_3O_4 were found to be superior heterogeneous catalysts to spherical polyhedral Fe_3O_4 NPs in terms of catalytic activity. Visible light irradiation of CuO/C/Fe_3O_4 photocatalyst increased the production of hydroxyl radicals ($^{\bullet}OH$), superoxide anion radicals ($^{\bullet}O_2^-$), and the redox Fe^{3+}/ Fe^{2+} pair, resulting in increased photodegradation performance. The present research demonstrated that the as-prepared CuO/C/Fe_3O_4 photocatalyst could be an efficient catalyst for wastewater remediation because of its ease of recoverability and excellent reusability.

Acknowledgments The authors (O. A. Alani, H. A. Ari, and N.-A. O. Offiong) are grateful to the Petroleum Technology Development Fund (PTDF) Nigeria for foreign research scholarship.

Author Contributions Conceptualization, OAA and WF; methodology, OAA and HAA; formal analysis, OAA; investigation, OAA; resources, WF; data curation, OAA; data interpretation, OAA, HAA, N.-A.O.O.; writing—original draft preparation, OAA; writing—review and editing, OAA, HAA, N.-A.O.O., SO.A. and WF; supervision, WF; funding acquisition, WF. All authors have read and agreed to the published version of the manuscript.

Funding Financial supports from the Natural Science Foundation of China (Grant no. 61774073), the Open Project of State Key Laboratory of Inorganic Synthesis and Preparative Chemistry, Jilin University (No. 2016-25), and the Science and Technology Development Program of Jilin Province, China (No. 20170101086JC) is also acknowledged.

Declarations

Conflict of interests The author declares that there is no conflict of interest.

References

Acedo-Mendoza AG, Infantes-Molina A, Vargas-Hernández D et al (2020) Photodegradation of methylene blue and methyl orange with CuO supported on ZnO photocatalysts: The effect of copper loading and reaction temperature. Mater Sci Semicond Process 119:105257. https://doi.org/10.1016/j.mssp.2020.105257

Alani OA, Ari HA, Offiong N-AO et al (2021) Catalytic removal of selected textile dyes using zero-valent copper nanoparticles loaded on filter paper-chitosan-titanium oxide heterogeneous support. J Polym Environ. https://doi.org/10.1007/s10924-021-02062-0

Benabbas K, Zabat N, Hocini I (2020) Facile synthesis of Fe3O4/CuO a core-shell heterostructure for the enhancement of photocatalytic activity under visible light irradiation. Environ Sci Pollut Res. https://doi.org/10.1007/s11356-020-10749-5

Cetinkaya SG, Morcali MH, Akarsu S et al (2018) Comparison of classic Fenton with ultrasound Fenton processes on industrial textile wastewater. Sustain Environ Res 28:165–170. https://doi.org/10.1016/j.serj.2018.02.001

Chai F, Li K, Song C, Guo X (2016) Synthesis of magnetic porous Fe3O4/C/Cu2O composite as an excellent photo-Fenton catalyst under neutral condition. J Colloid Interface Sci 475:119–125. https://doi.org/10.1016/j.jcis.2016.04.047

Chauhan M, Kaur N, Bansal P et al (2020) Proficient Photocatalytic and Sonocatalytic Degradation of Organic Pollutants Using CuO Nanoparticles. J Nanomater. https://doi.org/10.1155/2020/6123178

Cheng X-L, Jiang J-S, Jiang D-M, Zhao Z-J (2014) Synthesis of Rhombic dodecahedral fe3o4 nanocrystals with exposed high-energy 110 facets and their peroxidase-like activity and lithium storage properties. J Phys Chem C 118:12588–12598. https://doi.org/10.1021/jp412661e

Coleman HM, Vimonses V, Leslie G, Amal R (2007) Degradation of 1,4-dioxane in water using TiO2 based photocatalytic and H2O2/UV processes. J Hazard Mater 146:496–501. https://doi.org/10.1016/j.jhazmat.2007.04.049

Cong S, Xu Y (2011) Explaining the high photocatalytic activity of a mixed phase TiO2: a combined effect of O2 and crystallinity. J Phys Chem C 115:21161–21168. https://doi.org/10.1021/jp2055206

Divya N, Bansal A, Jana AK (2013) Photocatalytic degradation of azo dye Orange II in aqueous solutions using copper-impregnated titania. Int J Environ Sci Technol 10:1265–1274. https://doi.org/10.1007/s13762-013-0238-8

Douglas JJ, Sevrin MJ, Stephenson CRJ (2016) Visible light photocatalysis: applications and new disconnections in the synthesis of pharmaceutical agents. Org Process Res Dev 20:1134–1147. https://doi.org/10.1021/acs.oprd.6b00125

Es'haghzade Z, Pajootan E, Bahrami H, Arami M (2017) Facile synthesis of Fe3O4 nanoparticles via aqueous based electro chemical route for heterogeneous electro-Fenton removal of azo dyes. J Taiwan Inst Chem Eng 71:91–105. https://doi.org/10.1016/j.jtice.2016.11.015

Feng J, Wang Y, Hou Y, Li L (2017) Hierarchical structured ZnFe2O4@RGO@TiO2 composite as powerful visible light catalyst for degradation of fulvic acid. J Nanoparticle Res. https://doi.org/10.1007/s11051-017-3842-6

Gao N, Lu Z, Zhao X et al (2016a) Enhanced photocatalytic activity of a double conductive C/Fe3O4/Bi2O3 composite photocatalyst based on biomass. Chem Eng J 304:351–361. https://doi.org/10.1016/j.cej.2016a.06.063

Gao N, Lu Z, Zhao X et al (2016b) Enhanced photocatalytic activity of a double conductive C/Fe3O4/Bi2O3 composite photocatalyst based on biomass. Chem Eng J 304:351–361. https://doi.org/10.1016/j.cej.2016.06.063

Ghasemi H, Aghabarari B, Alizadeh M et al (2020) High efficiency decolorization of wastewater by Fenton catalyst: Magnetic iron-copper hybrid oxides. J Water Process Eng 37:101540. https://doi.org/10.1016/j.jwpe.2020.101540

Guo W, He H, Zhu H et al (2019) Preparation and properties of a biomass cellulose-based colorimetric sensor for Ag+ and Cu2+. Ind Crops Prod 137:410–418. https://doi.org/10.1016/j.indcrop.2019.05.044

Hasmath Farzana M, Meenakshi S (2014) Synergistic effect of chitosan and titanium dioxide on the removal of toxic dyes by the photodegradation technique. Ind Eng Chem Res 53:55–63. https://doi.org/10.1021/ie402347g

Hassan MM, Carr CM (2021) Biomass-derived porous carbonaceous materials and their composites as adsorbents for cationic and anionic dyes: A review. Chemosphere 265:129087. https://doi.org/10.1016/j.chemosphere.2020.129087

Jalaludin S, Arifin SA, Saleh R (2015) Magnetic composite Fe3O4/CuO/TiO2 nanoparticles: preparation, characterization and photocatalytic activity. Mater Sci Forum 827:13–18. https://doi.org/10.4028/www.scientific.net/MSF.827.13

Jiao C, Wang Y, Li M et al (2016) Synthesis of magnetic nanoporous carbon from metal-organic framework for the fast removal of organic dye from aqueous solution. J Magn Magn Mater 407:24–30. https://doi.org/10.1016/j.jmmm.2016.01.031

Juang R-S, Yei Y-C, Liao C-S et al (2018) Synthesis of magnetic Fe3O4/activated carbon nanocomposites with high surface area

as recoverable adsorbents. J Taiwan Inst Chem Eng 90:51–60. https://doi.org/10.1016/j.jtice.2017.12.005
Kshirsagar J, Shrivastava R, Adwani P (2017) Preparation and characterization of copper oxide nanoparticles and determination of enhancement in critical heat flux. Therm Sci 21:233–242. https://doi.org/10.2298/tsci140619026k
Kumar A, Rana A, Sharma G et al (2019) Recent advances in nano-Fenton catalytic degradation of emerging pharmaceutical contaminants. J Mol Liq 290:111177. https://doi.org/10.1016/j.molliq.2019.111177
Legrini O, Oliveros E, Braun AM (1993) Photochemical processes for water treatment. Chem Rev 93:671–698. https://doi.org/10.1021/cr00018a003
Li K, Zhao Y, Janik MJ et al (2017) Facile preparation of magnetic mesoporous Fe 3 O 4 /C/Cu composites as high performance Fenton-like catalysts. Appl Surf Sci 396:1383–1392. https://doi.org/10.1016/j.apsusc.2016.11.170
Lucas M, Peres J (2007) Degradation of reactive Black 5 by Fenton/UV-C and Ferrioxalate/H2O2/Solar light processes. Dye Pigment - Dye Pigment 74:622–629. https://doi.org/10.1016/j.dyepig.2006.04.005
Maia CG, Oliveira AS, Saggioro EM, Moreira JC (2014) Optimization of the photocatalytic degradation of commercial azo dyes in aqueous TiO2 suspensions. React Kinet Mech Catal 113:305–320. https://doi.org/10.1007/s11144-014-0737-8
Nguyen XS, Zhang G, Yang X (2017) Mesocrystalline Zn-Doped Fe3O4 hollow submicrospheres: formation mechanism and enhanced photo-fenton catalytic performance. ACS Appl Mater Interfaces 9:8900–8909. https://doi.org/10.1021/acsami.6b16839
Phan TTN, Nikoloski AN, Bahri PA, Li D (2018) Heterogeneous photo-Fenton degradation of organics using highly efficient Cu-doped LaFeO3 under visible light. J Ind Eng Chem 61:53–64. https://doi.org/10.1016/j.jiec.2017.11.046
Qian X, Ren M, Fang M et al (2018) Hydrophilic mesoporous carbon as iron(III)/(II) electron shuttle for visible light enhanced Fenton-like degradation of organic pollutants. Appl Catal B Environ 231:108–114. https://doi.org/10.1016/j.apcatb.2018.03.016
Qin L, Ru R, Mao J et al (2020) Assembly of MOFs/polymer hydrogel derived Fe3O4-CuO@hollow carbon spheres for photochemical oxidation: freezing replacement for structural adjustment. Appl Catal B Environ 269:118754. https://doi.org/10.1016/j.apcatb.2020.118754
Reza KM, Kurny A, Gulshan F (2017) Parameters affecting the photocatalytic degradation of dyes using TiO2: a review. Appl Water Sci 7:1569–1578. https://doi.org/10.1007/s13201-015-0367-y
Sakar M, Balakumar S, Saravanan P, Bharathkumar S (2016) Particulates vs. fibers: dimension featured magnetic and visible light driven photocatalytic properties of Sc modified multiferroic bismuth ferrite nanostructures. Nanoscale 8:1147–1160. https://doi.org/10.1039/C5NR06655G
Santoso E, Ediati R, Kusumawati Y et al (2020) Review on recent advances of carbon based adsorbent for methylene blue removal from waste water. Mater Today Chem 16:100233. https://doi.org/10.1016/j.mtchem.2019.100233
Shao Y, Gao Y, Yue Q et al (2020) Degradation of chlortetracycline with simultaneous removal of copper (II) from aqueous solution using wheat straw-supported nanoscale zero-valent iron. Chem Eng J 379:122384. https://doi.org/10.1016/j.cej.2019.122384
Sharma K, Raizada P, Hosseini-Bandegharaei A et al (2020) Fabrication of efficient CuO / graphitic carbon nitride based heterogeneous photo-Fenton like catalyst for degradation of 2, 4 dimethyl phenol. Process Saf Environ Prot 142:63–75. https://doi.org/10.1016/j.psep.2020.06.003
Shi X, Tian A, You J et al (2018) Degradation of organic dyes by a new heterogeneous Fenton reagent - Fe2GeS4 nanoparticle. J Hazard Mater 353:182–189. https://doi.org/10.1016/j.jhazmat.2018.04.018
Sum OSN, Feng J, Hub X, Yue PL (2005) Photo-assisted fenton mineralization of an azo-dye acid black 1 using a modified laponite clay-based Fe nanocomposite as a heterogeneous catalyst. Top Catal 33:233–242. https://doi.org/10.1007/s11244-005-2532-2
Sun X, Gao G, Yan D, Feng C (2017) Synthesis and electrochemical properties of Fe 3 O 4 @MOF core-shell microspheres as an anode for lithium ion battery application. Appl Surf Sci 405:52–59. https://doi.org/10.1016/j.apsusc.2017.01.247
Sun B, Li H, Li X et al (2018) Degradation of organic dyes over fenton-like Cu2O-Cu/C catalysts. Ind Eng Chem Res 57:14011–14021. https://doi.org/10.1021/acs.iecr.8b02697
Takai ZI, Mustafa MK, Asman S, Sekak KA (2019) Preparation and characterization of magnetite (Fe3O4) nanoparticles by sol-gel method. Int J Nanoelectron Mater 12:37–46
Tatarchuk T, Al-Najar B, Bououdina M, Ahmed MAA (2018) Catalytic and Photocatalytic Properties of Oxide Spinels. In: Martínez LMT, Kharissova OV, Kharisov BI (eds) Handbook of Ecomaterials. Springer International Publishing, Cham, pp 1–50
Taylor-Pashow KML, Della Rocca J, Xie Z et al (2009) Postsynthetic modifications of iron-carboxylate nanoscale metal–organic frameworks for imaging and drug delivery. J Am Chem Soc 131:14261–14263. https://doi.org/10.1021/ja906198y
Tian H, Fan H, Dong G et al (2016) NiO/ZnO p–n heterostructures and their gas sensing properties for reduced operating temperature. RSC Adv 6:109091–109098. https://doi.org/10.1039/C6RA19520B
Trogadas P, Fuller TF, Strasser P (2014) Carbon as catalyst and support for electrochemical energy conversion. Carbon NY 75:5–42. https://doi.org/10.1016/j.carbon.2014.04.005
Uthirakumar P, Devendiran M, Kim TH et al (2020) Fabrication of flexible sheets of Cu/CuO/Cu2O heterojunction nanodisks: A dominant performance of multiple photocatalytic sheets under natural sunlight. Mater Sci Eng B Solid-State Mater Adv Technol 260:114652. https://doi.org/10.1016/j.mseb.2020.114652
Wang ZL (2000) Transmission electron microscopy of shape-controlled nanocrystals and their assemblies. J Phys Chem B 104:1153–1175. https://doi.org/10.1021/jp993593c
Wang W, Serp P, Kalck P, Faria JL (2005) Visible light photodegradation of phenol on MWNT-TiO2 composite catalysts prepared by a modified sol–gel method. J Mol Catal A Chem 235:194–199. https://doi.org/10.1016/j.molcata.2005.02.027
Woan K, Pyrgiotakis G, Sigmund W (2009) Photocatalytic Carbon-Nanotube–TiO2 Composites. Adv Mater 21:2233–2239. https://doi.org/10.1002/adma.200802738
Wu Q, Siddique MS, Yu W (2021) Iron-nickel bimetallic metal-organic frameworks as bifunctional Fenton-like catalysts for enhanced adsorption and degradation of organic contaminants under visible light: kinetics and mechanistic studies. J Hazard Mater 401:123261. https://doi.org/10.1016/j.jhazmat.2020.123261
Xiao W, Jiang X, Liu X et al (2021) Adsorption of organic dyes from wastewater by metal-doped porous carbon materials. J Clean Prod 284:124773. https://doi.org/10.1016/j.jclepro.2020.124773
Xu R, Bi H, He G et al (2014) Synthesis of Cu-Fe3O4@graphene composite: a magnetically separable and efficient catalyst for the reduction of 4-nitrophenol. Mater Res Bull 57:190–196. https://doi.org/10.1016/j.materresbull.2014.05.045
Yang K, Peng H, Wen Y, Li N (2010) Re-examination of characteristic FTIR spectrum of secondary layer in bilayer oleic acid-coated Fe 3 O 4 nanoparticles. Appl Surf Sci 256:3093–3097. https://doi.org/10.1016/j.apsusc.2009.11.079
Yao Y, Lu F, Zhu Y et al (2015) Magnetic core-shell CuFe2O4@C3N4 hybrids for visible light photocatalysis of Orange II. J Hazard Mater 297:224–233. https://doi.org/10.1016/j.jhazmat.2015.04.046

Yin G, Nishikawa M, Nosaka Y et al (2015) Photocatalytic carbon dioxide reduction by copper oxide nanocluster-grafted niobate nanosheets. ACS Nano 9:2111–2119. https://doi.org/10.1021/nn507429e

You J, Guo Y, Guo R, Liu X (2019) A review of visible light-active photocatalysts for water disinfection: Features and prospects. Chem Eng J 373:624–641. https://doi.org/10.1016/j.cej.2019.05.071

Yu X, Lin X, Feng W, Li W (2018) Effective removal of tetracycline by using bio-templated synthesis of TiO 2 / Fe 3 O 4 heterojunctions as a UV – Fenton catalyst. Catal Lett. https://doi.org/10.1007/s10562-018-2544-8

Yu X, Lin X, Feng W, Li W (2019a) Effective removal of tetracycline by using bio-templated synthesis of TiO 2 /Fe 3 O 4 heterojunctions as a UV–Fenton catalyst. Catal Lett 149:552–560. https://doi.org/10.1007/s10562-018-2544-8

Yu X, Lin X, Li W, Feng W (2019b) Effective removal of tetracycline by using biochar supported Fe3O4 as a UV-Fenton catalyst. Chem Res Chinese Univ 35:79–84. https://doi.org/10.1007/s40242-018-8213-z

Zhang YF, Qiu LG, Yuan YP et al (2014) Magnetic Fe3O4@C/Cu and Fe3O4@CuO core-shell composites constructed from MOF-based materials and their photocatalytic properties under visible light. Appl Catal B Environ 144:863–869. https://doi.org/10.1016/j.apcatb.2013.08.019

Zhao W, Wang Y, Yang Y et al (2012a) Carbon spheres supported visible-light-driven CuO-BiVO 4 heterojunction: Preparation, characterization, and photocatalytic properties. Appl Catal B Environ 115–116:90–99. https://doi.org/10.1016/j.apcatb.2011.12.018

Zhao W, Wang Y, Yang Y et al (2012b) Carbon spheres supported visible-light-driven CuO-BiVO4 heterojunction: preparation, characterization, and photocatalytic properties. Appl Catal B Environ 115–116:90–99. https://doi.org/10.1016/j.apcatb.2011.12.018

Zhou Q, Wang Y, Xiao J, Fan H (2017) Fabrication and characterisation of magnetic graphene oxide incorporated Fe3O4@polyaniline for the removal of bisphenol A, t-octyl-phenol, and α-naphthol from water. Sci Rep. https://doi.org/10.1038/s41598-017-11831-8

Zhu H, Xiao L, Jiang R et al (2011) Efficient decolorization of azo dye solution by visible light-induced photocatalytic process using SnO2/ZnO heterojunction immobilized in chitosan matrix. Chem Eng J 172:746–753. https://doi.org/10.1016/j.cej.2011.06.053

Zhu Z, Lu Z, Wang D et al (2016) Construction of high-dispersed Ag/Fe3O4/g-C3N4 photocatalyst by selective photo-deposition and improved photocatalytic activity. Appl Catal B Environ 182:115–122. https://doi.org/10.1016/j.apcatb.2015.09.029

Zhu G, Yu X, Xie F, Feng W (2019) Ultraviolet light assisted heterogeneous Fenton degradation of tetracycline based on polyhedral Fe3O4 nanoparticles with exposed high-energy 110 facets. Appl Surf Sci 485:496–505. https://doi.org/10.1016/j.apsusc.2019.04.239

Authors and Affiliations

O. A. Alani[1] · H. A. Ari[1,2] · S. O. Alani[3] · N.-A. O. Offiong[1,4] · W. Feng[1]

✉ W. Feng
weifeng@jlu.edu.cn

N.-A. O. Offiong
no.offiong@topfaith.edu.ng

[1] Key Laboratory of Groundwater Resource and Environment, Ministry Education, College of New Energy and Environment, Jilin University, Changchun 130021, People's Republic of China

[2] Faculty of Science, National Open University of Nigeria, Lagos, Nigeria

[3] Science Laboratory Department, Nigeria Institute of Leather and Science Technology, Zaria, Kaduna State, Nigeria

[4] Department of Chemical Sciences, Faculty of Computing and Applied Sciences, Topfaith University, Mkpatak, Nigeria